

## A statistical model to explain the gamma-ray variability and flares of the Crab nebula

QIANG YUAN<sup>1</sup>, PENG-FEI YIN<sup>1</sup>, XUE-FENG WU<sup>2,3</sup>, XIAO-JUN BI<sup>1</sup>, SIMING LIU<sup>4</sup>, BING ZHANG<sup>5</sup>

<sup>1</sup>Key Laboratory of Particle Astrophysics, Institute of High Energy Physics, Chinese Academy of Sciences, Beijing 100049, China

<sup>2</sup>Purple Mountain Observatory, Chinese Academy of Sciences, Nanjing 210008, China

<sup>3</sup>Joint Center for Particle Nuclear Physics & Cosmology (J-CPNPC), Nanjing 210093, China

<sup>4</sup>Key Laboratory of Dark Matter and Space Astronomy, Purple Mountain Observatory, Chinese Academy of Sciences, Nanjing 210008, China

<sup>5</sup>Department of Physics and Astronomy, University of Nevada Las Vegas, Las Vegas, NV 89154, USA

yuanq@mail.ihep.ac.cn

**Abstract:** Recently the AGILE and Fermi/LAT detectors uncovered giant  $\gamma$ -ray flares from the Crab nebula. The duration of these flares is a few days. The Fermi/LAT data with monthly time binning further showed significant variability of the synchrotron tail of the emission, while the inverse Compton component was stable. The simultaneous or follow-up observations in X-ray, optical, infrared and radio bands did not find significant flux variation. Based on these observations, we propose that the  $\gamma$ -ray variability and flares are due to statistical fluctuations of knots that can accelerate electrons to  $\sim$ PeV energies. The maximum achievable energy of electrons is adopted to be proportional to the size of the knot, which is assumed to follow a power-law distribution. Thus the low energy electron flux will be stable due to the large number of small knots, while the high energy electron flux may experience large fluctuations. Monte Carlo realization of such a picture can reproduce the observational data quite well given proper model parameters.

**Keywords:** gamma rays: general — ISM: individual objects (Crab) — radiation mechanisms: non-thermal

## 1 Introduction

The Crab nebula is one of the most famous source in the sky, and is the most typical multi-band laboratory. It has been widely studied in all wavelengths, from radio to very high energy (VHE)  $\gamma$ -rays. The broadband non-thermal emission can be well modeled with a leptonic scenario, with the synchrotron radiation from the radio to GeV  $\gamma$ -rays and inverse Compton (IC) radiation above  $\sim$ GeV [1]. The transition from synchrotron to IC component was clearly seen by CGRO/EGRET [2] and Fermi/LAT [3]. Two populations of electrons, i.e., the radio electrons and wind electrons are required to fit the data [1]. The overall emission from the nebula seems to be stable in radio, optical, X-ray and VHE  $\gamma$ -ray bands, thus it was thought to be a “standard candle” and was often used to calibrate the detectors.

However, years ago people began to find that the MeV-GeV emission of Crab nebula was actually variable instead of stable, from the COMPTEL and EGRET observations [4, 5]. Furthermore the detailed images of the Crab nebula in optical and X-ray bands also indicated dynamical structures at small scales. The HST observation revealed highly variable wisps and knots in the nebula [6]. X-ray observations by ROSAT and Chandra uncovered a jet-torus

structure of the inner nebula, which was also dynamically variable [6, 7]. Recently in September 2010, the AGILE X-ray satellite detected a  $\gamma$ -ray flare above 100 MeV from Crab nebula, with a flux enhancement of  $\sim$  3 times higher than the average one and a duration of about 3 days [8]. This flare was confirmed by the Fermi/LAT detector, with an even higher flux enhancement [9]. The search for the archive data of AGILE and Fermi/LAT further unveiled other flares, in October 2007 for AGILE and in February 2009 for Fermi/LAT [8, 9], which may indicate that such flare events occur with a timescale about one year. Most recently in April 2011, AGILE detector observed another super-flare from Crab nebula [10]. Furthermore the monthly binned light curve of Fermi/LAT data showed that the synchrotron component is variable, however, no variation was found for the high energy IC component [9].

There were many other simultaneous or follow-up observations for the flare in September 2010 in other wavelength bands. In the VHE  $\gamma$ -ray energies, ARGO-YBJ collaboration reported a detection of a flux enhancement around TeV with a possibly longer duration (ATel #2921). The results from MAGIC and VERITAS telescopes with limited exposure time, however, did not find any flux variation during the flare phase (ATel #2967, #2968). In X-ray, optical, infrared and radio bands, no significant flux enhancement

was discovered either (ATel #2856, #2858, #2866, #2867, #2868, #2872, #2882, #2889, #2893, #2903).

Some theoretical models are proposed to explain the flare event [11, 12]. In [13] we proposed that the  $\gamma$ -ray variability and flare were due to the statistical fluctuation of the acceleration units which were responsible for the highest energy electrons. It is natural to expect that events that can generate the highest energy electrons are rarer, and therefore would suffer from the largest fluctuations. The lower energy electron spectrum should be steady-like because many more accelerators can contribute to them simultaneously. Since the synchrotron  $\gamma$ -rays are produced by the highest energy electrons ( $\sim$ PeV), while the synchrotron emission at lower energies and IC emission at higher energies are produced by lower energy electrons, we can easily explain why we only detect variability in MeV-GeV  $\gamma$ -rays, neither in lower nor in higher bands.

## 2 Model

We assume that electrons are accelerated in a series of knots, which may relate with the magnetic hydro-dynamic turbulence of the plasma. For each knot the output energy spectrum of electrons is a power-law function  $F_i(E) \propto E^{-\alpha_e}$  with a maximum electron energy  $E_{\max}^i$ , which is proportional to the size of the  $i$ th knot. It is further assumed that the size of knots has a power-law distribution  $P(r_i) \propto r_i^{-\beta}$ . The total electron spectrum can be got through adding the contribution from all the knots together.

The comoving system synchrotron spectrum from a knot with size  $r_i$  is  $\nu' F_{\nu'} \propto \nu'^{-\alpha_\nu} \exp(-\nu'/\nu'_{\max})$ , where  $\nu'_{\max} \propto (E_{\max}^i)^2 \propto r_i^2$ , and  $\alpha_\nu = (\alpha_e - 3)/2$  is the synchrotron spectral index, with  $\alpha_e$  being the power-law index of the electron distribution. Changing to the observer's frame, there will be a frequency shift  $\nu' \rightarrow \delta\nu'$  and a flux enhancement  $F_{\nu'} \rightarrow \delta^3 F_{\nu'}$ , where  $\delta$  is the Doppler factor of the knot.

It was shown that the maximal energy of synchrotron emission in the magnetic field dominated acceleration regime is  $\sim 70$  MeV, which is due to the fact that the electron may lose most of its energy in one cycle of the Larmor motion [14]. For smaller accelerators, the maximum energy is further limited by the size of the accelerator. The observational flare of Crab nebula has energies higher than GeV, which means that either there is Doppler boost of the flare event, or the acceleration of the electrons is not the shock-like scenario [9]. In order to explain the high energy photons of the flare event, we therefore employ a mild Doppler boost factor. Only knots with large enough size and large enough Doppler factor can contribute to high energy synchrotron radiation to explain the flares observed by Fermi/LAT.

The cooling of the electrons need to be considered. The cooling time of the electrons is energy dependent. For synchrotron photon with energy  $\epsilon$  the cooling time is  $t_c \simeq 1.5(B/\text{mG})^{-1.5}(\epsilon/\text{keV})^{-0.5}\delta^{-0.5}$  yr. If we adopt an av-

erage magnetic field of the Crab nebula  $B \approx 0.1$  mG, a mildly Doppler factor  $\delta \sim 1$ , the electrons correspond to  $\epsilon \sim 2.5$  eV photons will have a cooling time comparable to the age of the nebula  $t_{\text{age}} \approx 10^3$  yr. If the production of the knots is continuous, the equilibrium electron spectral index should be<sup>1</sup>  $\alpha_e = \alpha_e^{\text{inj}} + 1$ , for electrons with cooling time shorter than  $t_{\text{age}}$ . For the electrons with lower energies, whose cooling time is even longer than the age of the nebula, there will be no cooling at all and the injection spectrum will keep unchanged. Here we will focus on the high energy part, e.g., the synchrotron spectra from X-ray to  $\gamma$ -ray band, we will take a cooled spectrum of electrons as input of the model.

## 3 Monte Carlo simulation

We realize the above picture by a Monte-Carlo simulation. The injection spectrum of electrons from the knots is adopted as  $\alpha_e^{\text{inj}} = 1.6$ , which corresponds to the fit to the radio-optical spectrum of the nebula [15]. After taking into account the cooling effect the electron spectrum is  $\alpha_e = 2.6$ . We directly generate the synchrotron spectrum instead of the electron spectrum. The corresponding synchrotron spectral index is then  $\alpha_\nu = -0.2$ . The maximum energy of the synchrotron photon in the knot comoving system is proportional to  $r_i^2$ . We normalize  $\nu'_{\max}$  of the largest knot(s) to be 55 MeV to account for the constraints of cooling effect during the acceleration. The normalization of the synchrotron emissivity from each knot is adopted a volume-proportional factor  $r_i^3$ . As for the Lorentz factors of the knots, we assume a Gaussian distribution with the mean value  $\Gamma = 2.0$  and a standard deviation  $\sigma = 0.25$ . Such a Lorentz factor is consistent with the upper limit of the typical velocity of the jet [9]. The angle  $\theta$  between the knot motion and the line-of-sight is assumed to be randomly distributed. For  $3\sigma$  range of  $\Gamma$  we find the Doppler factor  $\delta = 1/\Gamma(1 - v \cos \theta)$  is in the range [0.18, 5.5]. Finally the power-law index of knot size distribution is adopted as  $\beta \approx 4.8$ . After adding the contribution from all the knots with different sizes together we get the total synchrotron spectrum  $\nu' F_{\nu'} \propto \nu'^{-0.2}$ , which can well reproduce the observed spectra of Crab nebula from optical to MeV  $\gamma$ -ray band, as shown in Figure 1.

The simulated spectra together with the observational data are shown in Figure 1. For comparison we show the fitting results to the broad band data with the thick blue line, with a broken power-law electron spectrum. The electron spectral indices are  $\beta_1/\beta_2 = 1.60/3.45$  below/above the break Lorentz factor  $\gamma_{\text{br}} = 1.1 \times 10^6$ . The high energy cutoff is adopted as a super-exponential behavior  $\gamma^{-\beta_2} \exp[-(\gamma/\gamma_{\text{cut}})^\delta]$ , with  $\gamma_{\text{cut}} = 5 \times 10^9$  and  $\delta = 2.0$ . The magnetic field  $B = 124 \mu\text{G}$ , which is a constant in the all nebula. This result is similar to the model invoking two population electrons as introduced in [1] and [15].

1. Note that here the equilibrium spectrum actually represents a series of knots with the same sizes, instead of a single one.

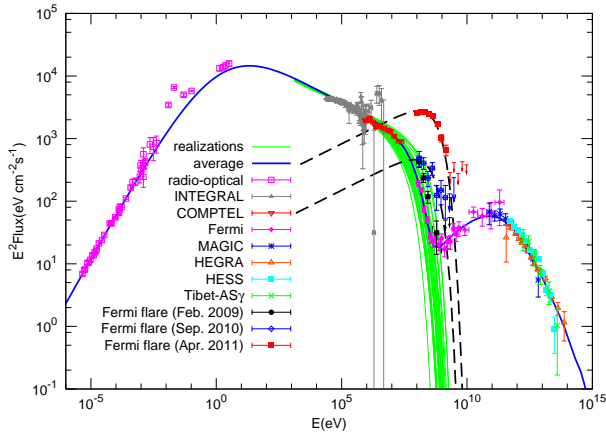


Figure 1: Spectral energy distribution of the Crab nebula. Thin-green-solid lines: simulated synchrotron spectra in 30 realizations; thick-blue-solid: fit of the average multi-wavelength emission; black-dashed: examples of unusual events which may be responsible for the flares. Data are from: radio-optical [16], INTEGRAL [17], COMPTEL [2], Fermi/LAT [3], MAGIC [18], HEGRA [19], HESS [20], Tibet-AS $\gamma$  [21], and Fermi/LAT flares [9, 22].

The average of the simulated spectra is similar to the steady state fit, and is consistent with the long term Fermi/LAT and COMPTEL data. However, there is scattering of the simulated spectra, which reflects the observational variability of the  $\gamma$ -ray spectrum. In the X-ray band, the fluctuation is very small, which is close to a steady state emission.

In this model, the IC component should not vary significantly. This is because the IC photons around TeV energies are primarily produced by the low energy electrons. For instance for  $\sim 100$  TeV electrons the synchrotron photon energy is typically  $0.016(B/\text{mG})(E/\text{TeV})^2 \text{ keV} \sim 16 \text{ keV}$  for  $B \sim 0.1 \text{ mG}$ , which suffers from very small fluctuation as shown in Figure 1. The corresponding IC photon energy is  $\epsilon_{\text{IC}} \sim \max(\gamma^2\epsilon, \gamma m_e)$ . For background photon energy  $\epsilon \sim \text{eV}$  the IC photon energy is as high as 100 TeV. Even for the cosmic microwave background photon  $\epsilon \sim 10^{-3} \text{ eV}$  we still have  $\epsilon_{\text{IC}} \sim 10 \text{ TeV}$ . Therefore the fluctuation of the IC component should be indeed small. This result is consistent with the Fermi/LAT observations [9].

The two large flares in September 2010 and April 2011 are not well reproduced in the simulation. We show two illustrations of these events with proper parameters in Figure 1. For the September 2010 flare the model parameters are  $\delta = 5.5$ ,  $\nu'_{\text{max}} = 70 \text{ MeV}$ . These parameters are reasonable in the present frame. However, for the April 2011 flare, we may need  $\delta = 8.0$ ,  $\nu'_{\text{max}} = 70 \text{ MeV}$ , which seem to be very extreme. Such a flare can be regarded as an event with very small probability.

To investigate the fluctuations of emission in detail, we calculate the light curves of the simulated photon fluxes. Since there is purely statistical fluctuation of the fluxes, we can adopt independent realizations to represent each time bin. The length of the time bin is proportional to the number of

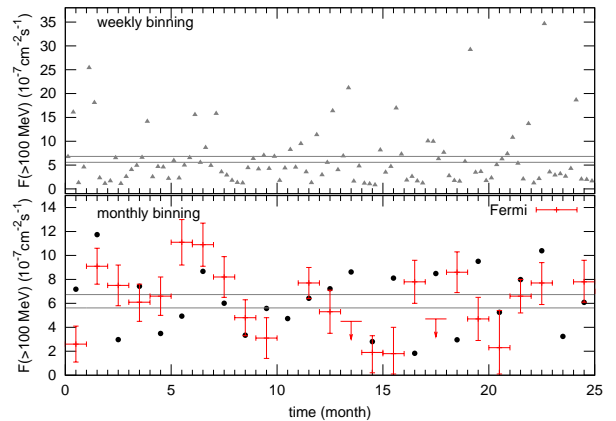


Figure 2: Light curves of the simulated synchrotron flux above 100 MeV. The upper panel shows the results with weekly bin and the bottom panel for monthly bin. The average flux of the realizations is normalized to the observational one  $\sim 6.2 \times 10^{-7} \text{ cm}^{-2} \text{ s}^{-1}$  [9], as shown with the horizontal lines. Also plotted in the lower panel are the Fermi/LAT observational data with monthly bin.

knots. We need a normalization of the absolute time scale, which is adopted that in one year there is an enhancement in flux by at least a factor of 5-6 for weekly bins, which may be responsible for a flare. We plot the weekly and monthly bin lightcurves in the upper and lower panels of Figure 2, respectively. The Fermi/LAT observed monthly light curve [9] is also plotted in the lower panel of Figure 2 for comparison. It can be seen that the predicted monthly variability scale of the simulated results is very similar to that observed by Fermi/LAT.

Figure 3 shows the histogram of the flux distribution. For the monthly bin results, we can see clearly the similarity between the simulation and the observational data. In the right panel of Figure 3 the histogram of flux distribution for weekly bin is shown. We can see that there is a significant concentration toward low-flux, which is distinct from a symmetric distribution around the average value. The detailed analysis of Fermi/LAT data can test such a prediction.

## 4 Conclusion

In this work we propose that the fluctuations of the electron spectra at the highest energy end ( $\sim \text{PeV}$ ) are responsible for the variability of the synchrotron tail in GeV  $\gamma$ -ray band. The electrons are thought to be accelerated in a series of knots, with a size distribution  $P(r_i) \propto r_i^{-\beta}$  and a distribution of the Doppler factor. The maximal achievable energy of the electrons in the co-moving frame is assumed to be proportional to the size of the knots. Thus the very high energy electrons are generated by the very rare knots with both large sizes and high Doppler boosts, and hence, suffer from large fluctuations. On the other hand, the low

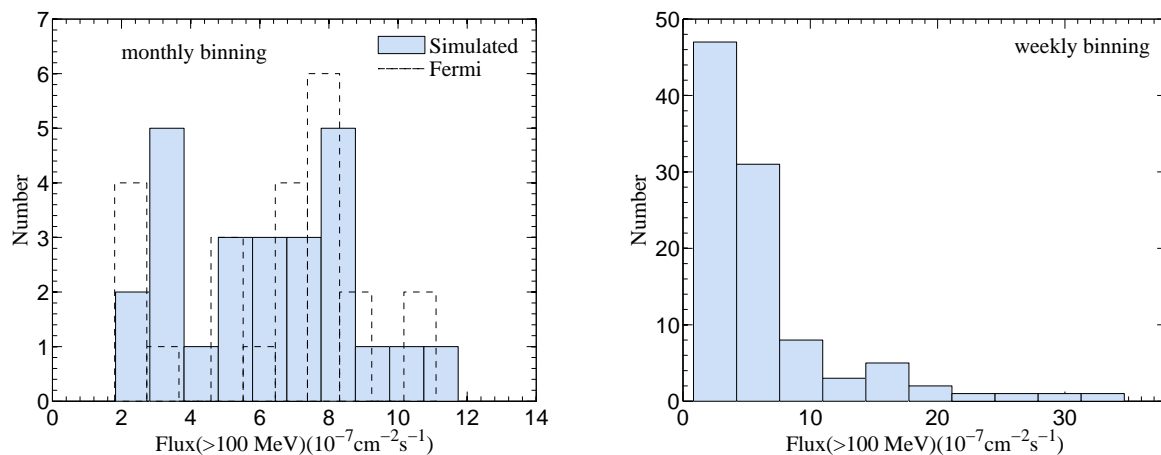


Figure 3: Histograms of the synchrotron flux distribution above 100 MeV, for monthly bin (left) and weekly bin (right), respectively. In the left panel the Fermi/LAT observation result is also shown (dashed histogram).

energy electrons can be accelerated by many smaller knots, and the fluctuations are smoothed out. Therefore only the variability in MeV-GeV  $\gamma$ -ray band is observed, because it is the direct reflection of the highest energy electrons. The lower energy synchrotron component and the higher energy IC component are relatively stable due to the less fluctuation of the low energy electrons. The expected variability of the monthly bin fluxes above 100 MeV are well consistent with that observed by Fermi/LAT. The two large  $\gamma$ -ray flares can also be naturally accounted for without additional assumptions.

It has been revealed recently that in the X-ray band the Crab nebula is actually no longer “standard candle”, but experiences quasi-periodic variability with a level of several percentage [25]. Such large scale variability may be due to the overall energy injection of the nebula or the inhomogeneous plasma flow induced magnetosonic waves [25]. The model proposed here may not be responsible for such variability. However, it would be interesting to investigate the statistical fluctuations of the X-ray fluxes in different energy ranges after removing the large scale variability, and compare with our model prediction.

One thing we should keep in mind is that in the present model we do not expect the variability of the IC component. This conclusion is consistent with the Fermi/LAT data, however, in a relatively long time scale (monthly bin). During the flare phase, we note that the ARGO-YBJ experiment detected a potential flux enhancement in TeV energy range (ATel #2921). Although it was not confirmed by the Cherenkov telescopes MAGIC (ATel #2967) and VERITAS (ATel #2968), we should note that the exposure time of MAGIC (1 hr) and VERITAS (2 hr) is very limited. It is thus very important to further monitor the Crab nebula in VHE energy band by e.g., Tibet-MD [23] or LHAASO [24], to search for the variability, which can be a crucial test of the current model.

This work is supported by the Natural Sciences Foundation of China grants 10773011, 11075169, 10633040

and 10921063, the 973 project grants 2010CB833000 and 2009CB824800, the NSF grant AST-0908362 and NASA grants NNX10AD48G and NNX10AP53G at UNLV.

## References

- [1] Atoyan, A. M., Aharonian, F. A., 1996, *MNRAS*, **278**, 525
- [2] Kuiper, L. et al., 2001, *A&A*, **378**, 918
- [3] Abdo, A. et al., 2010, *ApJ*, **708**, 1254
- [4] Much, R. et al., 1995, *A&A*, **299**, 435
- [5] de Jager, O. C. et al., 1996, *ApJ*, **457**, 253
- [6] Hester, J. J. et al., 1995, *ApJ*, **448**, 240
- [7] Weisskopf, M. C. et al., 2000, *ApJ*, **536**, L81
- [8] Tavani, M. et al., 2011, *Science*, **331**, 736
- [9] Abdo, A. et al., 2011, *Science*, **331**, 739
- [10] Striani, E. et al., ArXiv e-prints:1105.5028
- [11] Komissarov, S. S., Lyutikov, M., 2011, *MNRAS*, **414**, 2017
- [12] Bednarek, W., Idec, W., 2011, *MNRAS*, **414**, 2229
- [13] Yuan, Q. et al., 2011, *ApJ*, **730**, L15
- [14] Blumenthal, G. R., Gould, R. J., 1970, *Reviews of Modern Physics*, **42**, 237
- [15] Meyer, M., Horns, D., Zechlin, H., 2010, *A&A*, **523**, A2
- [16] Macias-Perez, J. F. et al., 2010, *ApJ*, **711**, 417
- [17] Jourdain, E., Roques, J. P., 2009, *ApJ*, **704**, 17
- [18] Albert, J. et al., 2008, *ApJ*, **674**, 1073
- [19] Aharonian, F. et al., 2004, *ApJ*, **614**, 897
- [20] Aharonian, F. et al., 2006, *A&A*, **457**, 899
- [21] Amenomori, M. et al., 2009, *ApJ*, **692**, 61
- [22] Buehler, R., Fermi Symposium, Roma 2011
- [23] Amenomori, M. et al., ArXiv e-prints:0710.2757
- [24] Cao, Z., 2010, *Chinese Physics C*, **34**, 249
- [25] Wilson-Hodge, C. A. et al., 2011, *ApJ*, **727**, L40